Causal propagation of nonanalytical points in fast- and slow-light media

Ryuta Suzuki and Makoto Tomita
Department of Physics, Faculty of Science, Shizuoka University, 836, Ohya, Suruga-ku, Shizuoka, 422-8529, Japan
(Received 4 September 2013; published 15 November 2013)

We examined the propagation of bending nonanalytical points encoded on temporally smooth Gaussian-shaped optical pulses in fast- and slow-light media, using an optical ring resonator. For bending nonanalytical points, the pulse function is continuous, but the first-order derivative is discontinuous, in contrast to traditional nonanalytical points in which the pulse function itself is discontinuous. The nonanalytical points were neither advanced nor delayed, but appeared at the same instance as they entered the ring resonator, in good accordance with the fact that the information velocity was equal to the light velocity in vacuum or the background medium. The differences between the traditional discontinuous and the present bending nonanalytical points were investigated.

DOI: 10.1103/PhysRevA.88.053822 PACS number(s): 42.25.Bs

I. INTRODUCTION

Fast and slow light have been attracting increasing interest where superluminal, negative, or extremely slow group velocities are achieved, through the control of quantum coherence in atoms and solids, or by manipulation of the photonic structure [1–3]. It is well established that the peak of Gaussian-shaped pulses travels at a speed predicted by the conventional definition of group velocity, even in superluminal propagation, as long as the propagation distance is sufficiently short [4–6]. In contrast to the peak, the front of the pulse always travels at the speed of light in vacuum, c, for both fast and slow light [7–9]. Sommerfeld and Brillouin analyzed the propagation of square-modulated pulses through a broad-bandwidth Lorentz medium under far-off-resonance conditions, and showed that the pulse breaks up into two small precursors before the arrival of the main signal. They also determined that the front of the Sommerfeld precursor always travels at c [7].

The information that can be encoded in an optical pulse has long been debated, especially for fast light. Conventionally, Brillouin defined signal velocity, v_s, as the velocity of the main body of the main pulse [7]. However, it is now accepted that true information is not contained in the pulse peak, but instead is encoded in nonanalytical points or singularities along the wave packets [10–15]. The arrival of the pulse peak or main body of a smooth superluminal pulse can be predicted using Taylor expansion of the leading part of the pulse. Hence, the pulse peak has no new information to add that is already present in the leading part of the pulse. Stenner *et al*. demonstrated that nonanalytical points encoded in the input pulses propagate at $v_i \approx c$ through fast-gain-assisted atoms [13] and through slow light in atomic systems [14], thereby proving that these signals propagate in a relativistically causal manner.

Nonanalytical points are not restricted to the front of the pulse or discontinuous points in the pulse envelope. Instead, nonanalytical points refer to points where discontinuities exist in the slope, or in any order of the derivatives [10]. Expansion cannot be applied relative to these points because the derivative is not defined. More work needs to be done on the propagation of optical pulses for which the function is continuous but the derivative is discontinuous.

Here, we examined the propagation of bending nonanalytical points encoded on temporally Gaussian-shaped optical pulses in fast- and slow-light systems using an optical ring resonator. The propagation of nonanalytical points can be interpreted as the information velocity [11–15]. Information velocity, an important concept in physics, preserves fundamental relativistic causality, and is important in practical applications because it determines the ultimate bit rate in information transfer through network systems. Experimental results have confirmed that the information velocity is equal to the velocity of light in vacuum or in the background medium, independent of the group velocity. The differences between the traditional discontinuous and the present bending nonanalytical points are also examined.

II. EXPERIMENTS

Figure 1 shows a schematic diagram of the experimental setup. In this study, we used a fiber ring resonator to control dispersion via cavity loss and coupling strength between the fiber and the ring resonator. The stationary input-output characteristics can be analyzed based on directional coupling theory [16]. The output light electric field, $E_{\mathrm{out}}(\omega)$, normalized by the incident light electric field, $E_{\mathrm{in}}(\omega)$, is given as

$$\frac{E_{\mathrm{out}}(\omega)}{E_{\mathrm{in}}(\omega)} = (1-\gamma)^{1/2}\left[\frac{y - x\exp(i\phi)}{1 - xy\exp(i\phi)}\right] = \sqrt{T(\omega)}\exp[i\theta(\omega)], \quad (1)$$

where $x = (1-\gamma)^{1/2}\exp(-\rho/2)$ and $y = \cos(\kappa)$ are the loss and coupling parameters, respectively, γ is the insertion loss, ρ is the round-trip loss, and κ is the coupling strength. $\phi(\omega) = n\omega L_R/c$ is the phase shift in the circulation orbit, where L_R represents the length of the ring resonator and n is the effective refractive index. The transmitted light intensity $T(\omega)$ as a function of ω shows a periodic dip structure due to resonances. The dispersion relationship depends on the loss and coupling strength. For the undercoupling condition, i.e., $x < y$, the transmission phase $\theta(\omega)$ as a function of frequency shows an anomalous dispersion at the center of the resonance, and the group delay is expected to be negative, $\tau_g = \partial\theta/\partial\omega < 0$, corresponding to superluminal pulse propagation. In contrast, when the coupling is strong, $x > y$, the transmission phase shows normal dispersion, and one would expect to observe slow light.

In the current study, 7:93 ($y^2 = 0.93$) and 40:60 ($y^2 = 0.6$) couplers were used to achieve under- and overcoupling

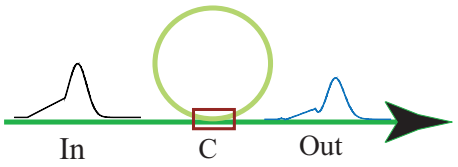

FIG. 1. (Color online) Experimental setup. The green circle represents the ring resonator. "C" corresponds to the coupler.

conditions, respectively. We inserted an additional loss element within the ring resonator to control the loss parameter. The physical length of the ring was $L_R = 220$ and 620 cm for the under- and overcoupling conditions, respectively. An Er-fiber laser was used as the incident light source. The spectral width was 1 kHz; the laser frequency was tuned by piezoelectric control of the cavity length. Nearly Gaussian temporal pulses were generated using a $LiNbO_3$ (LN) modulator. The typical temporal duration of the pulses was $t_p = 470$ ns [full width at half maximum (FWHM)]; shorter pulses were also used to adjust the bandwidth effect. The repetition rate was 100 kHz, and the incident power was 0.1 mW. The nonanalytical points were encoded on either the leading or trailing sides of Gaussian-shaped pulses. Transmission intensity through the

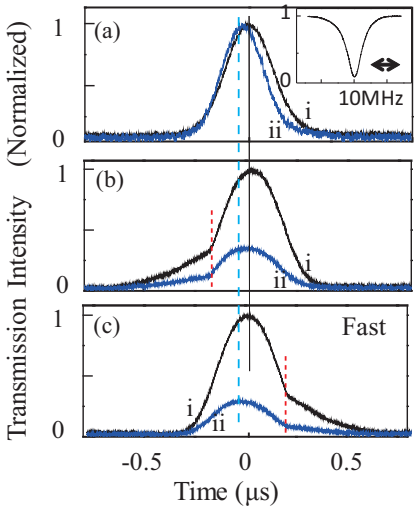

FIG. 2. (Color online) Experimental observations of the transmitted temporal pulse profiles in the fast-light system. (a) The upper right inset shows the transmission spectrum as a function of detuning frequency. In the main panel, the black and blue lines denoted by "i" and "ii" represent the input and output pulses, respectively. The input pulses were original Gaussian-shaped pulses. The pulse heights were normalized with respect to each other to show the peak advancement clearly. In (b) and (c), the input pulses were Gaussian-shaped pulses encoded with bending nonanalytical points on the leading and trailing edges, respectively. The black and blue lines denoted by "i" and "ii" represent the input and output pulses, respectively. The pulse heights were normalized by that of the input pulses. The vertical solid black line represents the peak time of the input pulses ($t = 0$) and the vertical dashed blue line represents the peak time of the output pulses. The dotted red lines in (b) and (c) represent the time when the bending nonanalytical points appeared.

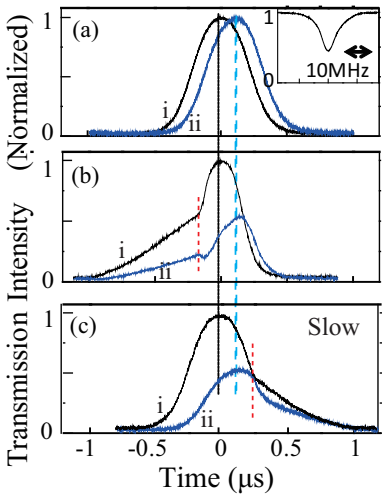

FIG. 3. (Color online) Similar plots as Fig. 2 for the slow-light system. (a) Original Gaussian-shaped pulses. (b) and (c) Gaussian-shaped pulses encoded with bending nonanalytical points on the leading and trailing edges, respectively. The notations "i" and "ii" and the vertical lines have the same meaning as those in Fig. 2.

system was observed using an InGaAs photodetector, and was reordered using a 600-MHz digital oscilloscope.

Figure 2 shows the transmitted temporal pulse profiles with bending nonanalytical points observed in the fast-light system using an undercoupled ring resonator. The upper right inset of Fig. 2(a) shows an example of the transmission spectrum as a function of the detuning frequency observed in continuous-wave mode, where the LN modulator was operated in open mode. The FWHM of the resonance dip was $\delta\nu_R = 5.8$ MHz. In the main frame of Fig. 2(a), the input pulses were Gaussian shaped. The pulse peak observed under the resonance condition $\delta\nu = 0$ was advanced $\tau = -39$ ns compared with the pulse peak observed under the off-resonance condition. This negative delay time was in good agreement with the expected delay time $\tau = -34$ ns from Eq. (1), demonstrating fast light in the undercoupled ring resonator. Figures 2(b) and 2(c) show the propagation of Gaussian-shaped pulses encoded with a bending nonanalytical point at time $t_{NA} = -175$ ns on the leading side, and $t_{NA} = 200$ ns on the trailing side, respectively. While the peaks were still advanced, the nonanalytical points were neither advanced nor delayed, but appeared at the same instance as they entered the ring resonator, in good accordance with the causal principle of information transfer in a fast-light system; i.e., the information velocity was equal to the speed of light in vacuum or in the background medium. Figure 3 shows similar experimental results for slow light in the overcoupled ring resonator. In Fig. 3(a), the pulse peak was delayed $\tau = 120$ ns compared with the pulse peak under off-resonance conditions. This delay time was also in good agreement with the expected delay time from Eq. (1). Figures 3(b) and 3(c) show the temporal profiles of the Gaussian-shaped pulses encoded with bending nonanalytical points on the leading and the trailing edges, respectively. Although the peaks were delayed, which reflected the normal dispersion in the system, the nonanalytical points were neither advanced nor delayed, but instead appeared at the same instance as entering the system. This indicated that the

information velocity was equal to the light velocity in vacuum or in the background medium, even in the slow-light medium.

III. DISCUSSION: TWO TYPES OF NONANALYTICAL POINTS

So far, we have experimentally demonstrated the causal propagation of bending nonanalytical points in fast- and slow-light systems. There are several items worth discussing. The traditional nonanalytical point (t_{NA}), at which the pulse function is discontinuous, is expressed as

$$\lim_{\varepsilon\to 0} E_{\rm in}(t_{NA}-\varepsilon) \neq \lim_{\varepsilon\to 0} E_{\rm in}(t_{NA}+\varepsilon). \tag{2}$$

In contrast, a bending nonanalytical point, at which the propagation function is continuous but the first-order derivative is discontinuous, may be defined as

$$\begin{aligned} &\lim_{\varepsilon\to 0} E_{\rm in}(t_{NA}-\varepsilon) = \lim_{\varepsilon\to 0} E_{\rm in}(t_{NA}+\varepsilon), \\ &\lim_{\varepsilon\to 0} \frac{\partial E_{\rm in}(t)}{\partial t}\bigg|_{t_{NA}-\varepsilon} \neq \lim_{\varepsilon\to 0} \frac{\partial E_{\rm in}(t)}{\partial t}\bigg|_{t_{NA}+\varepsilon}. \end{aligned} \tag{3}$$

For pulse propagation in dispersive media, a convenient analytic form to represent the outgoing pulses within the group-velocity approximation is given by Ref. [11] as

$$E_{\rm out}(t,z) = \frac{1}{2\pi}\exp\left[z\left(\frac{1}{c}-\frac{1}{v_g}\right)\frac{\partial}{\partial t}\right]E_{\rm in}\left(t-\frac{z}{c}\right). \tag{4}$$

Equation (4) states that propagation over a distance z corresponds to an analytic continuation over time, $z/c - z/v_g$, of the vacuum-propagated pulse envelope, $E_{\rm in}(t-z/c)$. Superluminal group velocity does not imply superluminal propagation of new information because the information in $E_{\rm out}(t,z) = E_{\rm in}(t-z/v_g)$ is already contained in $E_{\rm in}(t-z/c)$. From Eqs. (2)–(4), it can be concluded that for both discontinuous and bending nonanalytical points,

$$\begin{aligned} &\lim_{\varepsilon\to 0} E_{\rm out}(t_{NA}+z/c-\varepsilon,z) \neq \lim_{\varepsilon\to 0} E_{\rm out}(t_{NA}+z/c+\varepsilon,z), \\ &\lim_{\varepsilon\to 0} \frac{\partial E_{\rm out}(t,z)}{\partial t}\bigg|_{t_{NA}+z/c-\varepsilon} \neq \lim_{\varepsilon\to 0} \frac{\partial E_{\rm out}(t,z)}{\partial t}\bigg|_{t_{NA}+z/c+\varepsilon}. \end{aligned} \tag{5}$$

Hence, the nonanalytical points propagate with a speed of c and not v_g, indicating that superluminal group velocity does not imply superluminal propagation of new information.

In the mathematical sense, the above discrimination between traditional discontinuos nonanalytical points and the present bending nonanalytical points is apparent. However, from a physical point of view, the difference may not be so clear. In any real physical system, the physical quantity should be "continuous," in that any real system requires a finite time to respond to the input signal. In quantum mechanics, however, the results of an observation may be discontinuous; for example, an observed result may be assigned "0" before the observation, before jumping to "1" the instant the observation is made. Even in quantized physics, however, the discontinuity appears only in an ideal observation, and the probability, or the wave function, develops continuously in unitary processes.

In real experiments, if we look into the details of the temporal profile with much higher time resolution, the pulse amplitude is continuous, even at the discontinuous nonanalytical point. However, in a realistic sense, the function

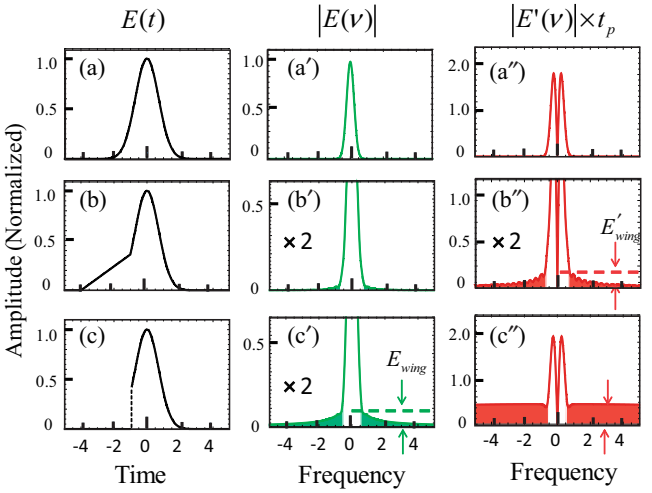

FIG. 4. (Color online) Distinction between traditional discontinuous and bending nonanalytical points in Fourier space. Left column: three types of input temporal profiles, $E(t)$: (a) original Gaussian-shaped pulses, and (b) and (c) Gaussian-shaped pulses encoded with the bending and discontinuous nonanalytical points, respectively. Middle column: (a′)–(c′) are the amplitudes of the Fourier components for the input pulses shown in (a)–(c), respectively. Right column: (a″)–(c″) are the amplitudes of the Fourier components for the first-order derivative of the input pulses shown in (a)–(c), respectively. The green-shaded region in (c′) and red-shaded regions in (b″) and (c″) are denoted to call attention to the wing Fourier components used to distinguish between the two types of nonanalytical points. The units for time and frequency are (t_e) and (t_e^{-1}), respectively.

can be recognized as discontinuous if the function changes much faster than the bandwidth of the dispersive system. In our experiments, the rise and fall time of the system was approximately 2.5 ns (400 MHz). In contrast, the bandwidth of the resonance of the present ring resonator was $\delta\nu_R =$ 5.8 MHz. Therefore, temporal structures that have higher Fourier components than 5.8 MHz could be recognized as nonanalytical for the present ring resonator. It may, therefore, be possible to discriminate two situations: one in which the function is discontinuous, and the other in which the function is continuous but its derivative is discontinuous.

Figure 4 illustrates a trial of this discrimination in Fourier space. The left column shows three types of input pulses, $E(t)$. Figure 4(a) shows the original Gaussian-shaped pulses. Figures 4(b) and 4(c) show Gaussian-shaped pulses encoded with bending and discontinuous nonanalytical points, respectively, at time $t_{NA} = -t_e$ on the leading side of the pulse, where $t_e = t_p/(2\sqrt{\ln 2})$ corresponds to the time at which the field amplitude becomes $1/e$ of the pulse peak. Figures 4(a′)–4(c′), are the amplitudes of the Fourier components, $|E(\nu)| = |\int dt[E(t)]e^{-i\omega t}|$, for the input pulses shown in (a)–(c), respectively. For the original Gaussian pulse, the Fourier components have only the central components, $E_{\rm center}$, with a width of $\sim t_e^{-1}$. In contrast, the pulses with a traditional discontinuous point [Fig. 4(c)′] have widespread Fourier component wings, $E_{\rm wing}$ [green-shaded region in (c′)]. The ratio of the wing components to the center component is $E_{\rm wing}/E_{\rm center} \sim 0.047$ in Fig. 4(c)′. The bending nonanalytical points in Fig. 4(b)′, however, contain only very little of the wing components;

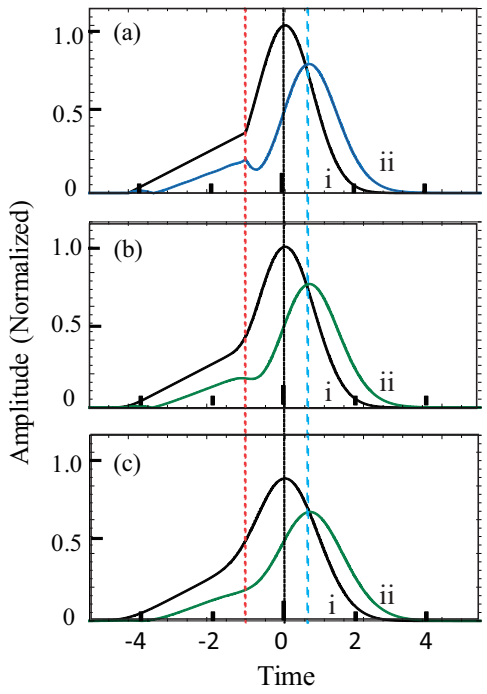

FIG. 5. (Color online) Effect of the finite spectral bandwidth of the incident pulses with respect to the bending point, in the slow-light system. (a) Original bending point. The black and blue lines denoted by "i" and "ii" represent the input and output pulses, respectively. (b) and (c) Bandwidth of the input pulse is restricted to $\Delta\nu_B \leqslant t_e^{-1}$ and $\Delta\nu_B \leqslant 0.5t_e^{-1}$, respectively. The black and green lines denoted by "i" and "ii" represent the bandwidth-restricted input and output pulses, respectively. The pulse heights were normalized by that of the original input pulse [panel (a) "i"]. The vertical solid black line represents the peak time of the input pulses ($t = 0$) and the vertical dashed blue line represents the peak time of the output pulses. The dotted red line represents the time when the bending points enter. The unit for time is (t_e).

$E_{\text{wing}}/E_{\text{center}} < 0.01$. Figures 4(a)″–4(c)″ show the amplitudes of the Fourier components for the first-order derivative of the input pulses, $|E'(\nu)| = |\int dt[dE(t)/dt]e^{-i\omega t}|$, in (a)–(c), respectively. In this case, not only the discontinuous nonanalytical point [Fig. 4(c)″], but also the bending nonanalytical point [Fig. 4(b)″] have wing Fourier components, E'_{wing} [red-shaded region in Figs. 4(b)″ and 4(c)″]. The ratios are $E'_{\text{wing}}/E'_{\text{center}} = 0.11$ and $E'_{\text{wing}}/E'_{\text{center}} = 0.23$ in Figs. 4(b)″ and 4(c)″, respectively. Therefore, the present bending nonanalytical point can be distinguished from the traditional discontinuous nonanalytical point as $E_{\text{wing}}/E_{\text{center}} < C$ and $E'_{\text{wing}}/E'_{\text{center}} > C$, where C is a critical value; for the case presented here, C was set to 0.01.

Although the wing Fourier components in the higher and lower frequency regions are small for the bending nonanalytical point [Fig. 4(b)′], these components are critically important for the propagation of nonanalytical points. The simulation shown in Fig. 5 demonstrates the propagation of the bending nonanalytical point, where the sharpness of the bend was changed using a band-pass filter. Figure 5(a) shows the propagation of the original bending point in the slow-light system, which corresponds to the experiment shown in Fig. 3(b). In this case, the bending point propagates with velocity c, while the pulse peak propagates with a positive delay time, τ_g; hence, a small dip appears in the transmitted pulse profile just after the bending point [Fig. 5(a)]. In contrast, in Figs. 5(b) and 5(c), the Fourier bandwidth of the input pulse, $\Delta\nu_B$, is filtered to restrictions $\Delta\nu_B \leqslant t_e^{-1}$ and $\Delta\nu_B \leqslant 0.5t_e^{-1}$, respectively. In Fig. 5(c), the dip is filled and the relatively smooth bending point propagates with the group delay τ_g, keeping a total pulse shape similar to that of the incident pulse. This point cannot be recognized as a nonanalytical point in this system.

IV. SUMMARY

In summary, we experimentally demonstrated that bending nonanalytical points encoded on smooth Gaussian-shaped optical pulses were neither advanced nor delayed, but appeared at the same instance as they entered the system. This observation indicates that the information velocity, as the propagation of nonanalytical points, is equal to the light velocity in vacuum or the background medium, in good accordance with the causal principle observed in a fast- and slow-light system. The bending nonanalytical points could be discriminated from traditional discontinuous nonanalytical points in Fourier space analysis.

[1] Focus issue: *Slow Light*, T. F. Krauss *et al.*, Nat. Photonics **2**, 447 (2008).
[2] Feature issue: *Slow Light and Its Applications*, R. W. Boyd *et al.* eds. J. Opt. Soc. Am. B **25**, C1 (2008).
[3] P. W. Milonmi, *Fast Light, Slow Light and Left-Handed Light* (Taylor & Francis, New York, 2004).
[4] S. Chu and S. Wong, Phys. Rev. Lett. **48**, 738 (1982).
[5] L. J. Wang, A. Kuzmich, and A. Dogariu, Nature **406**, 277 (2000).
[6] A. I. Talukder, Y. Amagishi, and M. Tomita, Phys. Rev. Lett. **86**, 3546 (2001).
[7] L. Brillouin, *Wave Propagation and Group Velocity* (Academic, New York, 1960).
[8] K. E. Oughstun and G. C. Sherman, *Electromagnetic Pulse Propagation in Causal Dielectrics* (Springer-Verlag, Berlin, 1994).
[9] N. Brunner, V. Scarani, M. Wegmuller, M. Legre, and N. Gisin, Phys. Rev. Lett. **93**, 203902 (2004).
[10] R. Y. Chiao and A. M. Steinberg, in *Progress in Optics XXXVII*, edited by E. Wolf (Elsevier, Amsterdam, 1997), p. 345.
[11] G. Diener, Phys. Lett. A **223**, 327 (1996).
[12] K. Wynne, Opt. Commun. **209**, 85 (2002).
[13] M. D. Stenner, D. J. Gauthier, and M. A. Neifeld, Nature (London) **425**, 695 (2003).
[14] M. D. Stenner, D. J. Gauthier, and M. A. Neifeld, Phys. Rev. Lett. **94**, 053902 (2005).
[15] M. Tomita, H. Uesugi, P. Sultana, and T. Oishi, Phys. Rev. A **84**, 043843 (2011).
[16] K. Totsuka, N. Kobayashi, and M. Tomita, Phys. Rev. Lett. **98**, 213904 (2007).